# Data-driven approaches for Tau-PET imaging biomarkers in Alzheimer's disease

Jacob W. Vogel, BA[1,2]*, Niklas Mattsson, MD, PhD[3,4,5], Yasser Iturria-Medina, PhD[1], T. Olof Strandberg, PhD[3], Michael Schöll, PhD[3,6], Christian Dansereau, PhD[7,8], Sylvia Villeneuve, PhD[1,9], Wiesje M. van der Flier, MA[2,10], Philip Scheltens, MD[2], Pierre Bellec, PhD[7,8], Alan C. Evans, PhD[1], Oskar Hansson, MD, PhD[3,4]#, Rik Ossenkoppele, PhD[2,3]#, the Alzheimer's Disease Neuroimaging Initiative** & the Swedish BioFINDER study

[1] Montreal Neurological Institute, McGill University, Montreal, QC, Canada
[2] Alzheimer Center and Department of Neurology, VU University medical center, Amsterdam Neuroscience, Amsterdam, Netherlands
[3] Clinical Memory Research Unit, Lund University, Lund, Sweden
[4] Memory Clinic, Skåne University Hospital, Lund, Sweden
[5] Department of Neurology, Skåne University Hospital, Lund, Sweden
[6] Wallenberg Centre for Molecular and Translational Medicine, University of Gothenburg, Gothenburg, Sweden
[7] Department of Computer Science and Operations research, Université de Montréal, Montreal, QC, Canada
[8] Centre de Recherche de l'Institut Universitaire de Gériatrie de Montréal, University of Montreal, Montreal, QC, Canada
[9] Department of Psychiatry, McGill University, Montreal, QC, Canada
[10] Department of Epidemiology and Biostatistics, VU University medical center, Amsterdam, Netherlands

# Both authors contributed equally to this work.

* Corresponding author
Jacob W. Vogel
jacob.vogel@mail.mcgill.ca
McGill Centre for Integrative Neuroscience
Montreal Neurological Institute, Room NW145
3801 Boulevard Robert-Bourassa
Montreal, QC H3A 2B4
Canada

** Data used in preparation of this article were obtained from the Alzheimer's Disease Neuroimaging Initiative (ADNI) database (adni.loni.usc.edu). As such, the investigators within the ADNI contributed to the design and implementation of ADNI and/or provided data but did not participate in analysis or writing of this report. A complete listing of ADNI investigators can be found at: http://adni.loni.usc.edu/wp-content/uploads/how_to_apply/ADNI_Acknowledgement_List.pdf

## ABSTRACT

Previous positron emission tomography (PET) studies have quantified filamentous tau pathology using regions-of-interest (ROIs) based on observations of the topographical distribution of neurofibrillary tangles in post-mortem tissue. However, such approaches may not take full advantage of information contained in neuroimaging data. The present study employs an unsupervised data-driven method to identify spatial patterns of tau-PET distribution, and to compare these patterns to previously published "pathology-driven" ROIs. Tau-PET patterns were identified from a discovery sample comprised of 123 normal controls and patients with mild cognitive impairment or Alzheimer's disease (AD) dementia from the Swedish BioFINDER cohort, who underwent [$^{18}$F]AV1451 PET scanning. Associations with cognition were tested in a separate sample of 90 individuals from ADNI. BioFINDER [$^{18}$F]AV1451 images were entered into a robust voxelwise stable clustering algorithm, which resulted in five clusters. Mean [$^{18}$F]AV1451 uptake in the data-driven clusters, and in 35 previously published pathology-driven ROIs, was extracted from ADNI [$^{18}$F]AV1451 scans. We performed linear models comparing [$^{18}$F]AV1451 signal across all 40 ROIs to several tests of global cognition, adjusting for age, sex and education. Two data-driven ROIs consistently demonstrated the strongest or near-strongest effect sizes across all cognitive tests. Inputting all regions plus demographics into a feature selection routine resulted in selection of two ROIs (one data-driven, one pathology-driven) and education, which together explained 28% of the variance of a global cognitive composite score. Our findings suggest that [$^{18}$F]AV1451-PET data naturally clusters into spatial patterns that are biologically meaningful and that may offer advantages as clinical tools.

## 1. INTRODUCTION

Alzheimer's disease (AD) is neuropathologically defined by the presence of widespread extracellular plaques containing amyloid-β and intracellular neurofibrillary tangles consisting of aggregated tau proteins [Braak and Braak, 1991; Masters et al., 1985]. While amyloid-β may be present decades prior to symptom onset [Jansen et al., 2015], the presence of neocortical tau is temporally more closely related to current cognitive status and degree of neurodegeneration, as convincingly demonstrated by studies utilizing post-mortem tissue, animal models, cerebrospinal fluid and, more recently, the positron emission tomography (PET) tracer [$^{18}$F]AV1451 [Arriagada et al., 1992; Bejanin et al., 2017; Cho et al., 2017; Nelson P. T. et al, 2013; Ossenkoppele et al., 2016; Van Rossum et al., 2012]. [$^{18}$F]AV1451 binds paired helical filaments of tau with high affinity and selectivity [Chien et al., 2013; Lowe et al., 2016; Marquié et al., 2015; Marquié et al., 2017; Xia et al., 2013], and can be used to investigate the distribution of tau pathology in the living human brain. Several studies have shown strong spatial resemblance between *in vivo* tau PET patterns and neuropathological staging of neurofibrillary tangles as proposed by Braak and Braak [Cho et al., 2016; Schöll et al., 2016; Schwarz et al., 2016], reflecting prototypical progression from (trans)entorhinal (stage I/II) to limbic (stage III/IV) to isocortical (stage V/VI) regions [Braak and Braak, 1991]. Furthermore, regional [$^{18}$F]AV1451 retention co-localizes with sites of brain atrophy or hypometabolism [Ossenkoppele et al., 2016; Xia et al., 2017] and has been associated with impairments in specific cognitive domains [Bejanin et al., 2017; Cho et al., 2017; Ossenkoppele et al., 2016].

88 Given this strong regional specificity of tau pathology, it is important to consider
89 how regions-of-interest (ROIs) are defined, as they could potentially impact study
90 outcomes. To date, most studies employing tau-PET tracers involved ROIs constructed
91 based on neuropathological studies. For example, some studies mimicked the Braak
92 stages *in* vivo [Cho et al., 2016; Schöll et al., 2016; Schwarz et al., 2016], while others
93 selected specific regions reflecting early (e.g. entorhinal cortex) or more advanced (e.g.
94 inferior temporal cortex) disease stages [Johnson et al., 2016]. These approaches have
95 several advantages as they are supported by fundamental research and enhance
96 generalizability across studies. However, compared to neuroimaging, neuropathological
97 data typically include only a few slices in a constrained number of brain regions, and
98 brain tissue is affected by death [Scheltens and Rockwood, 2011]. Additionally, tau PET
99 signal does not equal presence of tau pathology. There are several sources of
100 [$^{18}$F]AV1451 signal and noise, including target binding, off-target binding (e.g.
101 Monamine oxidase, neuromelanin, vascular lesions, iron), non-specific binding and
102 imaging related noise (e.g. partial volume effects) [Choi et al., 2017; Harada et al., 2017;
103 Ikonomovic et al.,; Lockhart et al., 2017; Lowe et al., 2016; Marquié et al., 2015; Ng et
104 al., 2017; Schöll et al., 2016]. An alternative approach could therefore be to select ROIs
105 based on data-driven approaches [Dickerson et al., 2011; Landau et al., 2011; Pankov et
106 al., 2016], thereby taking full advantage of the abundance of information contained in
107 neuroimaging data, but also accounting the idiosyncrasies of PET imaging data.

108 In light of ongoing efforts to define appropriate ROIs and determine tau PET-
109 positivity, it is important to compare data-driven approaches (agnostic, "where is the
110 tau?") with theory-derived ROIs based on post-mortem studies (directed, "is the tau

111 here?"). In the present study, we applied an unsupervised algorithm to identify clusters of
112 [$^{18}$F]AV1451 signal. We then compared the spatial patterns of these clusters with
113 neuropathologically derived ROIs described in previous publications. Finally, we tested
114 which ROI best correlated with global cognition in an independent cohort of cognitively
115 normal, mild cognitive impairment and AD dementia subjects. We hypothesized that our
116 data-driven approach would corroborate neuropathological findings, but would also
117 present novel information leading to enhanced associations with cognition.
118

119 ## 2. MATERIALS AND METHODS

120 ### 2.1 Participants

121 Two separate cohorts were included in this study. Participants from the Swedish
122 BioFINDER study were used to perform clustering analysis on [$^{18}$F]AV1451 data,
123 whereas participants from the Alzheimer's Disease Neuroimaging Initiative (ADNI) were
124 used to test associations between the clustering-derived ROIs and cognition.
125 Demographic, clinical and biomarker information for both cohorts are presented in Table
126 1.

127 The BioFINDER cohort is a multi-site study designed for the purpose of
128 developing biomarkers for neurodegenerative diseases. More information can be found at
129 http://biofinder.se. Study participants included 55 subjects with normal cognition, 21 with
130 (MCI), and 47 with Alzheimer's dementia, who had complete MRI and [$^{18}$F]AV1451
131 PET data (Table 1). Patients with MCI were referred to a memory clinic and
132 demonstrated objective cognitive impairment that could not be explained by another
133 condition. AD dementia patients met criteria for the DSM-V [American Psychiatric

134 Association, 2013] and NINCDS-ADRDA [McKhann et al., 2011] for probable AD,
135 established by clinicians blinded to PET data. To optimize overlap with the ADNI cohort,
136 dementia patients were only included if they presented with an amnestic-predominant
137 phenotype. Both dementia and MCI patients were only included in this study if they
138 demonstrated abnormal Aβ1-42 levels in the CSF (INNOTEST, cut-off: 650 ng/l;
139 Palmqvist *et al.*, 2015). The sample of controls selected for [$^{18}$F]AV1451 scanning was
140 intentionally enriched for β-amyloid positivity to include people in the preclinical stage
141 of AD (see Table 1). PET imaging for the study was approved by the Swedish Medicines
142 and Products Agency and the local Radiation Safety Committee at Skåne University
143 Hospital, Sweden. All participants provided written informed consent according to the
144 Declaration of Helsinki, and ethical approval was given by the Ethics Committee of Lund
145 University, Lund, Sweden.
146 ADNI is a multi-site open source dataset designed to accelerate the discovery of
147 biomarkers to identify and track AD pathology [Weiner et al., 2012]. The current study
148 included all ADNI individuals with complete [$^{18}$F]AV1451 scans that were available in
149 November, 2016. This included 43 cognitively normal elderly controls, 37 patients with
150 MCI, and 10 patients with a recent diagnosis of Alzheimer's dementia (Table 1).
151 In addition to imaging data, age, sex, education, diagnosis, amyloid-β status on
152 [$^{18}$F]florbetapir PET [Landau et al., 2013], and scores from six tests measuring global
153 cognition or activities of daily living were downloaded from the ADNI-LONI website
154 (adni.loni.usc.edu). The cognitive tests were as follows: Mini-Mental State Examination
155 (MMSE) [Folstein et al., 1975]; Clinical Dementia Rating Sum of Boxes (CDRSB)
156 [Hughes et al., 1982]; Alzheimer's disease Assessment Scale 11 (ADAS11) [Rosen et al.,

1984] and 13 (ADAS13) [Mohs et al., 1997]; Everyday Cognition (ECog) [Farias et al., 2008]; Functional Activities Questionnaire (FAQ) [Pfeffer et al., 1982].

## 2.2 Imaging

[$^{18}$F]AV1451 images were processed using separate but nearly identical pipelines across the two cohorts. Acquisition and processing procedures for [$^{18}$F]AV1451 processing in the BioFINDER cohort has been described elsewhere [Hansson et al., 2017]. Scans were reconstructed into 5-min frames and motion corrected using AFNI's 3dvolreg https://afni.nimh.nih.gov/. Mean [$^{18}$F]AV1451 images were created over a time-window of 80-100 minutes post-injection, and these images were coregistered to each subject's T1 image in native space. Mean images were then intensity normalized using a complete cerebellar gray reference region to create standard uptake value ratio (SUVR) images. Coregistered MRI images were normalized to the MNI-ICBM152 template using Advanced Normalization Tools (https://stnava.github.io/ANTs/) and the transformation parameters were applied to the SUVR images. Finally, SUVR images were smoothed with an 8mm FWHM Gaussian filter.

For the ADNI cohort, mean 80-100 min [$^{18}$F]AV1451 images, as well as MPRAGE images closest to [$^{18}$F]AV1451 scans, were downloaded from the ADNI-LONI website. Details on acquisition procedures for these [$^{18}$F]AV1451 and MRI images can be found elsewhere (http://adni.loni.usc.edu/methods/documents/). [$^{18}$F]AV1451 images were processed in accordance to procedures described in [Schöll et al., 2016]. Briefly, T1 images were processed using Freesurfer v5.3 and [$^{18}$F]AV1451 images were coregistered to native T1s using Statistical Parametric Mapping 12 (www.fil.ion.ucl.ac.uk/spm/).

180 SUVR images were created using a cerebellar gray reference region and images were
181 normalized to MNI space using the parameters from the coregistered T1. Figure 1 shows
182 mean [$^{18}$F]AV1451 SUVR images stratified by diagnosis and amyloid status for each
183 cohort.
184

185 **2.3 Clustering of [$^{18}$F]AV1451 data**

186 Cross-subject [$^{18}$F]AV1451-PET covariance networks were derived from all 123
187 BioFINDER [$^{18}$F]AV1451 images using an open-source unsupervised consensus-
188 clustering algorithm called Bootstrap Analysis of Stable Clusters (BASC; Figure 2)
189 [Bellec et al., 2010]. The algorithm was adapted to 3D [$^{18}$F]AV1451 data by stacking all
190 123 BioFINDER [$^{18}$F]AV1451 images along a fourth (subject) dimension, creating a
191 single 4D image to be submitted as input. BASC first reduces the dimensions of the data
192 with a previously described region-growing algorithm [Bellec et al., 2006], which was set
193 to extract spatially constrained atoms (small regions of redundant signal) with a size
194 threshold of 1000mm$^3$. In order to reduce computational demands, the Desikan-Killainy
195 atlas [Desikan et al., 2006] was used as a prior for region constraint, and the data was
196 masked with a liberal gray matter mask, which included the subcortex but had the
197 cerebellum manually removed (since this was used as the reference region for
198 [$^{18}$F]AV1451 images). The region-growing algorithm resulted in a total of 730 atoms,
199 which were included in the BASC algorithm. BASC next performs recursive k-means
200 clustering on bootstrapped samples of the input data. After each clustering iteration,
201 information about cluster membership is stored as a binarized adjacency matrix. The
202 adjacency matrices are averaged resulting in a stability matrix representing probabilities

of each pair of atoms clustering together (Figure 2). Finally, hierarchical agglomerative clustering with Ward criterion is applied to the stability matrix, resulting in the final clustering solution. The process is repeated over several clustering solutions (k=1 - 50), and the MSTEPs method [Bellec, 2013] was implemented to find the most stable clustering solutions at different resolutions. In the interest of multiple comparisons, and similarity to Braak neuropathological staging (i.e. six ROIs), we chose the lowest resolution solution for subsequent analysis. Note that no size constraints were imposed on clustering solutions. Voxels were only included in a cluster when cluster probability membership exceeded 0.5 (BASC default setting), eliminating unstable voxels from analysis [Bellec et al., 2010; Garcia-Garcia et al., 2017]. After determining clusters in the BIOFINDER cohort, we extracted the (size-weighted) average [$^{18}$F]AV1451 SUVR for each cluster from all ADNI subjects, and these values were used for subsequent analysis investigating associations with cognition.

BASC was chosen over other clustering algorithms because its bootstrapping feature offers two advantages in the context of this study. First, the stochastic nature of many clustering algorithms tends to lead to different solutions depending on their initialization state, whereas BASC performs clustering on a stability matrix generated from many solutions (and thus many initializations). This leads to greater reproducibility in the clustering solutions generated by BASC. Second, because the initial set of clustering analyses is performed on bootstrap samples of the input data, the final solution is less dependent on the clinical composition of the input data.

## 2.4 Definition of Braak stage ROIs described in other studies

226 A number of studies have created ROIs mirroring the Braak stages described from
227 pathological studies. To test the utility of our data-driven ROIs vis-à-vis those defined in
228 correspondence to the pathological literature, we recreated the Braak ROIs described in
229 three different studies [Cho et al., 2016; Schöll et al., 2016; Schwarz et al., 2016]. Schöll,
230 Lockhart et al. and Cho et al. were constructed using regions from the Desikan-Killainy
231 atlas, and we recreated these ROIs in direct correspondence to what has been reported in
232 these two studies. Schwarz et al. instead generated small ROIs designed to mirror the
233 slabs of cerebral cortex extracted during autopsy for Braak staging. These regions were
234 constructed with a script generously provided by the authors. For all analyses, Braak
235 ROIs were included both individually ("single") and cumulatively ("stage"). For
236 example, for Braak Stage III, one ROI was created containing all regions from Braak I,
237 II, and III included ("stage"), as well as a ROI created including only regions in Braak III
238 ("single"). Finally, some studies have chosen to use only the bilateral inferior temporal
239 lobe from the Desikan-Killainy atlas to summarize global tau burden [Johnson et al.,
240 2016], so we included this region in subsequent analysis as well. Studies also frequently
241 used the bilateral entorhinal cortex from this atlas, and it should be noted that this region
242 is also included, namely as Stage I from Cho et al. and Schöll, Lockhart et al. Size-
243 weighted average [$^{18}$F]AV1451 SUVR was extracted for each ROI (35 in total) for each
244 subject.
245

246 **2.5 Similarity between data-driven clusters, anatomical ROIs and Braak**
247 **Stage ROIs**

We compiled descriptive information about the similarity between our cluster-derived ROIs and the Braak ROIs from the literature. For comparisons to regions from Schöll, Lockhart et al. and Cho et al., we used normalized mutual information. Due to the small size of the Schwarz et al. regions, comparisons involved measuring the percentage of each Schwarz ROI falling inside of each cluster-derived ROI.

## 2.6 Statistical Analysis

In order to test the utility of our data-driven covariance networks, we performed linear models between these covariance networks and the scores from six different available test scores assessing global cognition and function (see Table 2). In addition, the scores were summarized using Principal Components Analysis (PCA) using Singular Value Decomposition. The PCA was fit to data from the six cognitive test scores, which were scaled to a 0 mean with unit variance. The first component explained 72% of the total model variance, and was used to transform the cognitive data into a single Global Cognition composite score. For each of the cognitive tests, as well as the composite score, separate general linear models for each ROI (40 in total; our five data-driven clusters and 35 ROIs from the literature) were constructed with cognitive test score as the dependent variable and age, sex and education as covariates. Tests surviving Bonferroni correction for multiple comparisons are reported.

In order to identify a sparse set of non-redundant covariates that best describe the global cognitive data in ADNI, we submitted all 40 tau ROIs plus age, sex and education to a Least Absolute Shrinkage and Selection Operator (Lasso) regression-based feature selection routine. The Lasso uses L1 regularization (coordinate descent) to penalize

regression coefficients based on their maximum likelihood estimates, and is therefore an optimal approach to select a small number of variables from a large number of collinear covariates. In the current implementation, the degree of penalization is optimized using 10-fold cross-validation. All tau ROIs and demographics were scaled to be mean-centered with unit variance, and entered into the Lasso regression model with the Global Cognition composite score as the dependent variable. Features selected by the Lasso (absolute beta > 0.25) were entered together into a general linear model (GLM) with MMSE as the dependent variable. Additionally, to ensure our results were representative of global cognition and not specific to the composite score, the fitted values from this GLM were used to predict scores of each of the six cognitive tests. Finally, the Lasso was repeated separately for each of the individual test as well.

With the exception of BASC, all statistics were implemented using the pandas, numpy, scipy and scikit-learn [Pedregosa et al., 2012] packages in Python 3.5.2 (https://www.python.org/).

# 3. RESULTS

## 3.1 Participant Characteristics

Table 1 contains demographic information, MMSE scores and amyloid positivity rates for both the ADNI and BioFINDER sample. The sample used for clustering (BioFINDER) demonstrated important differences compared to the sample used for testing (ADNI). BioFINDER subjects were less highly educated across the whole sample, and BioFINDER controls were on average older than ADNI controls. Additionally, the BioFINDER sample demonstrated lower MMSE scores across the whole sample

294 compared to ADNI, including within MCI and dementia groups. Finally, 45% of ADNI
295 subjects were amyloid-positive vs. 73% of BioFINDER subjects, which was primarily
296 related to the fact that only amyloid positive MCI patients were included in the
297 BioFINDER sample.
298

299 **3.2 Data-driven Tau-PET covariance networks**

300 123 BioFINDER [$^{18}$F]AV1451 scans were entered into an advanced clustering
301 algorithm in order to identify networks of regional [$^{18}$F]AV1451 signal covariance across
302 subjects. The M-STEPS algorithm identified five-, nine- and 32-cluster solutions as
303 optimal solutions. For the purposes of comparing with Braak stage ROIs, we chose the
304 lowest-resolution solution (n=5) for subsequent analyses, visualized in Figure 2. The
305 clusters were interpreted and named as follows: "1: Subcortical", "2: Frontal", "3:
306 Medial/Anterior/Inferior Temporal", "4: Temporo-parietal" and "5: Unimodal Sensory".
307 Cluster 3 bore resemblance to regions often involved in early tau aggregation and atrophy
308 [Braak and Braak, 1991], while Cluster 4 also appeared similar to regions commonly
309 associated with neurodegeneration in AD [Dickerson et al., 2011; Landau et al., 2011].
310 Of note, the hippocampus was largely unrepresented in any of the cluster-cores, though
311 some voxels in the head of the hippocampus were included in Cluster 3, and a few
312 distributed voxels were included in Cluster 1 (Subcortex). However, using a winner-
313 takes-all clustering approach, the majority the hippocampal voxels clustered with other
314 subcortical and periventricular regions.
315

316 **3.3 Similarity to Braak ROIs**

Descriptive metrics were used to quantify the spatial similarity between the data-driven covariance networks and the Braak Stage ROIs introduced in the literature (Figure 3). Cluster 5 ("Unimodal Sensory") demonstrated a high degree of overlap with Braak Stage VI across all region sets. Spatial similarity was also evident between Cluster 3 ("Medial/Anterior/Inferior Temporal") and Stage I-IV from Cho et al., and this cluster almost completely circumscribed Stages I-III from Schwarz et al. Cluster 1 ("Subcortex") was most similar to Schöll, Lockhart et al. Stage II, due in part to its inclusion of the hippocampus. Little spatial similarity was evident between Cluster 2 ("Frontal") and any of the Braak Stage ROIs, though some similarity was seen with the Stage V region from Schöll, Lockhart et al. and Cho et al. due to their inclusion of many frontal lobe structures. Similarly, Cluster 4 ("Temporo-parietal") did not demonstrate strong spatial similarity to any of the Braak ROIs, though it did partially overlap with the Braak Stage VI and Stage V regions from Schwarz et al.

### 3.4 Associations with global cognition in ADNI

General linear models were run in the ADNI dataset assessing associations separately between each of 40 tau ROIs (our five data-driven clusters established in the BioFINDER study, and 35 ROIs from the literature) and a Global Cognitive composite score, controlling for age, sex and education (Figure 4). AV1451 signal in several ROIs demonstrated strong associations with global cognition, though only the data-driven Cluster 4 ("Temporo-parietal"; $\beta = -3.24$ [SE=0.91], $t = -3.43$, $p<0.001$) survived multiple comparisons.

To ensure our results were not specific to the Global Cognition composite score, we repeated this analysis using the six individual measures of global cognition and function that composed the composite score (Table S1). The data-driven Cluster 4 ("Temporo-parietal") described global cognition better than all other ROIs using four of the six cognitive measures, and was in the top five for all of them. Across all cognitive measures, Clusters 4 and 3 ("Medial/anterior/inferior temporal") ranked best and second best, respectively, at describing global cognitive data (Figure 5). Notably, the Schwarz Stage I ROI also performed well across cognitive measures, except for the MMSE.

### 3.5 Identifying a combinatorial tau-PET biomarker for cognition

Next, all tau ROIs were entered into a Lasso regression model in order to identify a sparse set of covariates that best describe global cognitive data (Figure 6). The optimal penalization value was defined through cross-validation as 0.019. The Lasso reduced all coefficients except Cluster 4 ("Temporo-parietal"), Braak Stage VI from Schwarz et al., and education. These three variables were entered together into a general linear model, and together explained a much greater proportion of variance in global cognitive data ($r^2[4:81] = 0.28$, $p<0.0001$; Figure 5) compared to the individual effect sizes of each covariate (highest $r^2 = 0.12$). The earlier negative association between Cluster 4 and Global Cognition was strengthened ($t=-4.98$, $p<0.001$), although positive associations were seen for the other two covariates (Schwarz Single 6: $t = 3.61$, $p = 0.001$; Education: $t = 2.53$, $p = 0.013$). In addition, the fitted values of this GLM explained 18.7 – 26.2% of the variance in the six individual cognitive tests composing the composite score (all $p <0.001$), indicating the model generalizes well to individual cognitive tests (Table S2).

362 Finally, the Lasso feature selection analysis was repeated for the six individual tests of
363 global cognition. The data-driven Cluster 4 was selected across all six analyses, and was
364 the only ROI selected for two analyses (Table S3).
365

366 **4. DISCUSSION**

367 In the present study, we applied an advanced unsupervised algorithm to identify
368 clusters of [$^{18}$F]AV1451 signal in 123 subjects ranging from cognitively normal to AD
369 dementia in the Swedish BioFINDER study. Our approach yielded clusters in the
370 temporoparietal, medial/inferior/anterior temporal, unimodal sensory and frontal cortex,
371 as well as the subcortex. In an independent sample of 90 subjects (ADNI), we performed
372 general linear models between tests of global cognition and each [$^{18}$F]AV1451 cluster,
373 adjusting for age, sex and education. In addition, we ran similar models using 35
374 neuropathologically derived ROIs from previous publications [Cho et al., 2016; Johnson
375 et al., 2016; Schöll et al., 2016; Schwarz et al., 2016]. Several ROIs exhibited strong
376 relationships with cognition, though certain data-driven clusters (temporoparietal and
377 medial/inferior/anterior temporal cortex) appeared to perform slightly but consistently
378 better than other ROIs in ADNI. Supporting this notion, the temporoparietal data-driven
379 cluster was among the three most important features (identified by a Lasso regression
380 model) for predicting global cognition scores. Unsupervised clustering of [$^{18}$F]AV1451
381 PET data thus revealed the data to self-assemble into ROIs resembling well described
382 vulnerable regions in AD, some of which actually enhanced description of cognitive data
383 in an independent dataset. This suggests that data-driven approaches to delineate ROIs
384 may improve clinical utility of [$^{18}$F]AV1451 PET data.

385 The tau-PET covariance networks derived from our clustering approach exhibited
386 a fair degree of overlap with Braak ROIs derived from autopsy studies, thereby
387 demonstrating biological relevance. Particularly, Cluster 3 ("Medial/Anterior/Inferior
388 Temporal") was reminiscent of regions involved in early tau accumulation, whereas
389 Cluster 5 ("Unimodal Sensory") demonstrated a high degree of similarity to regions
390 involved only in the latest stages of AD. In contrast, Cluster 4 ("Temporo-parietal") did
391 not strongly resemble any of the Braak regions, while its pattern, together with the pattern
392 of cluster 3, spatially overlapped with cortical regions most vulnerable to
393 neurodegeneration in AD [Dickerson et al., 2011; Landau et al., 2011]. Furthermore,
394 signal in the hippocampus was heterogenous, adding additional evidence that
395 [$^{18}$F]AV1451 signal in this structure should be interpreted with caution [Cho et al., 2016]
396 [Choi et al., 2017; Ikonomovic et al.,]. Similarly, our data-driven approach suggested that
397 most (but not all) frontal lobe structures exhibited [$^{18}$F]AV1451 signal patterns unique to
398 the rest of the cortex. This is notable considering the original Braak Stage V aggregates
399 frontal lobe structures with many of the temporo-parietal structures captured in our
400 Cluster 4. Part of the successful description of cognitive data by the data-driven ROI may
401 be due to its isolation from many of these frontal lobe structures, which may be
402 contributing signal less informative to AD progression, particularly in early disease
403 stages. Finally, our data-driven ROIs provide information that may reconcile some
404 differences between existing Braak ROIs. For example, in our study, [$^{18}$F]AV1451 signal
405 in the putamen and insula covaried with other regions involved in early tau accumulation,
406 which was similar to the ROIs described by Schöll, Lockhart et al., but not Cho et al. (see
407 Table S4 for a summary).

408 Despite the clusters being derived from a sample with several important and
409 disease-relevant differences compared to the testing sample, these data-driven ROIs
410 described global cognitive data slightly better than regions derived from autopsy studies.
411 While the improvement over the other regions was subtle, the increasing movement
412 toward the development of biomarkers demands optimization of ROIs to summarize
413 [$^{18}$F]AV1451 signal [Frisoni et al., 2017; Maass et al., 2017; Mishra et al., 2017]. As
414 such, even small improvements are important for studies assessing more subtle effects of
415 cortical tau accumulation and studies seeking optimal biomarkers for multimodal
416 classification or disease progression [Ota et al., 2015]. The improvement observed is
417 likely due to the data-driven nature of the method used for derivation of the clusters.
418 [$^{18}$F]AV1451 may be binding to several off-target agents, such as (neuro)melanin, iron,
419 vascular pathology and MAO-A/B [Choi et al., 2017; Lowe et al., 2016; Marquié et al.,
420 2015; Ng et al., 2017], and as such, [$^{18}$F]AV1451 signal is likely a mix of true tau
421 pathology and other off-target and non-specific signals. Deriving the clusters from a
422 sample representing a wide breadth of disease stages and additionally including subjects
423 unlikely to have significant cortical tau pathology enhances the likelihood of isolating
424 true tau signal, which covaries strongly and in a regionally specific pattern across disease
425 stages. Additionally, deriving the clusters voxelwise allows freedom from anatomical
426 borders, which may impose unnecessary constraints irrelevant to the spread of tau.
427 Finally, despite its many limitations, multi-subject automatic whole-brain sampling is a
428 distinct advantage of [$^{18}$F]AV1451-PET over pathological studies. This advantage may
429 further enhance the efficacy of data-driven approaches to ROI generation, which evaluate
430 regions equally that may otherwise be overlooked.

431 The results of this study thus suggest a possible advantage of data-driven
432 approaches in evaluating [$^{18}$F]AV1451 PET data as a biomarker for AD. This study adds
433 to a rapidly growing body of data-driven [$^{18}$F]AV1451-PET studies that have helped to
434 characterize features of this tracer in the context of AD. Sepulcre and colleagues
435 employed a similar unsupervised clustering approach on a set of cognitively intact elderly
436 individuals, which, similar to our study, revealed [$^{18}$F]AV1451-PET covariance between
437 regions of early- and later- stage tau accumulation [Sepulcre et al., 2017]. This suggests
438 these patterns of signal covariance are stable even in the earliest disease stages, lending
439 credence to the use of data-driven biomarkers in multiple contexts. Meanwhile, Jones et
440 al. used a data-driven Independent Components Analysis approach to summarize
441 [$^{18}$F]AV1451 data [Jones et al., 2017]. While the authors concluded the resulting ROIs
442 represented functional brain networks, three of the ROIs bore a striking similarity to
443 those generated by our clustering approach. Our approach builds on these previous
444 studies by assessing relationships between data-driven ROIs and cognition, and by
445 comparing them with other existing ROIs. Maass et al. employed a series of *a priori* and
446 supervised data-driven methods to generate [$^{18}$F]AV1451 ROIs and found a relative
447 equivalence between these ROIs in their association with cognition and a number of other
448 disease markers [Maass et al., 2017]. However, consistent with our study, Maass et al.
449 found [$^{18}$F]AV1451 signal to covary most strongly within a specific set of AD
450 vulnerable-regions, and conclude that these regional measures may perform better than
451 whole-brain ROIs, particularly regarding associations with cognition.
452 We employed a widely used feature selection routine to identify those regions
453 most informative in describing association between [$^{18}$F]AV1451 signal and cognitive

data. The feature most strongly associated with global cognition was the data-driven temporo-parietal cluster, which harbored a strong negative relationship when included with the other selected features ($p<0.001$). The feature selection also resulted in the selection of Schwarz et al. Stage VI and education, both of which associated positively with MMSE in a general linear model. The finding of an association between education and MMSE controlling for tau pathology is consistent with the concept of cognitive reserve [Stern, 2012], and suggests that more highly educated subjects may experience preserved cognition in the face of tau pathology [Hoenig et al., 2017]. While the selection of Schwarz Stage VI is less obvious, possible explanations include partial volume effects and age-related off-target or non-specific signal. Because very few ADNI subjects demonstrate strong [$^{18}$F]AV1451 signal in this ROI, higher [$^{18}$F]AV1451 signal may be related to the presence of more cortex (and thus more off-target or non-specific binding) rather than increased tau pathology. Similarly, off-target [$^{18}$F]AV1451 signal in the cortex and subcortex has been shown to increase with age [Choi et al., 2017; Schöll et al., 2016; Smith et al., 2016], possibly representing binding to reactive astrocytes [Harada et al., 2017] or iron deposits [Choi et al., 2017]. Since age was not selected by the Lasso and therefore was not included in the multivariate model, this may explain the positive association between these regions and global cognition when accounting for AV1451 signal in the temporoparietal region. However, the fact that these ROIs were selected instead of age suggests they may carry additional cognition-relevant information, which may demand further exploration. Regardless, the negative relationship between Cluster 4 ("Temporo-parietal") and global cognition was substantially increased after regressing

476 out these other variables. This suggests that [$^{18}$F]AV1451-cognition relationships may be
477 enhanced by regressing out off-target or non-specific signal sources.
478 Our study comes with a number of limitations. First, there were several
479 differences in characteristics between the two samples. We decided to use the
480 BioFINDER cohort for clustering given the broad range of both [$^{18}$F]AV1451 uptake
481 (Figure 1) and cognitive scores (Table 1). As a consequence, validation of the clusters
482 was performed in subjects from the ADNI cohort with more restricted [$^{18}$F]AV1451
483 uptake and cognitive scores. On a related note, our cluster and results could be influenced
484 by the composition of our samples. However, voxels are only included in the clusters
485 derived for our analysis if the clustering occurs across >50% of bootstrap samples, so it is
486 unlikely that the clustering solution would be strongly driven by, for example, the high
487 proportion of late-stage (i.e. AD) subjects in the BioFINDER sample. Third, contrary to
488 other studies, we did not make an attempt to classify individuals according to stages of
489 tau pathology. Finally, we chose not to apply partial volume correction on our data.
490 Investigating the impact of such corrections is certainly important, but we were interested
491 in the natural behavior of tau-PET signal before any corrections.
492 In order to aid future studies, we have made the [$^{18}$F]AV1451 clusters from this
493 study available on FigShare (doi = 10.6084/m9.figshare.5758374).
494
495

496 **Acknowledgements**

497 Work at the authors' research centers was supported by the European Research Council,
498 the Swedish Research Council, the Strategic Research Area MultiPark (Multidisciplinary

499 Research in Parkinson's disease) at Lund University, the Swedish Brain Foundation, the
500 Swedish Alzheimer Association, the Marianne and Marcus Wallenberg Foundation, the
501 Skåne University Hospital Foundation, and the Swedish federal government under the
502 ALF agreement. This research was additionally funded by Marie Curie FP7 International
503 Outgoing Fellowship [628812] (to R.O.); The donors of [Alzheimer's Disease Research],
504 a program of BrightFocus Foundation (to R.O.); Author JWV was additionally funded by
505 an Alzheimer Nederland grant and a Vanier Canada Graduate Studies Doctoral award.
506 The authors would like to thank Emma Wolters, Tessa Timmers, Colin Groot, Angela
507 Tam, Alle Meije Wink and Elena Kochova for advice and support. The authors would
508 additionally like to thank Adam Schwarz for providing scripts to recreate the ROIs from
509 Schwarz et al., 2016, and Chul Hyoung Lyoo for providing information about creating
510 ROIs from Cho et al., 2016. AVID Radiopharmaceutical generously provided the
511 precursor of AV-1451. Data collection and sharing for this project was funded in part by the
512 Alzheimer's Disease Neuroimaging Initiative (ADNI) (National Institutes of Health Grant U01 AG024904)
513 and DOD ADNI (Department of Defense award number W81XWH-12-2-0012). ADNI is funded by the
514 National Institute on Aging, the National Institute of Biomedical Imaging and Bioengineering, and through
515 generous contributions from the following: AbbVie, Alzheimer's Association; Alzheimer's Drug Discovery
516 Foundation; Araclon Biotech; BioClinica, Inc.; Biogen; Bristol-Myers Squibb Company; CereSpir, Inc.;
517 Eisai Inc.; Elan Pharmaceuticals, Inc.; Eli Lilly and Company; EuroImmun; F. Hoffmann-La Roche Ltd
518 and its affiliated company Genentech, Inc.; Fujirebio; GE Healthcare; IXICO Ltd.; Janssen Alzheimer
519 Immunotherapy Research & Development, LLC.; Johnson & Johnson Pharmaceutical Research &
520 Development LLC.; Lumosity; Lundbeck; Merck & Co., Inc.; Meso Scale Diagnostics, LLC.; NeuroRx
521 Research; Neurotrack Technologies; Novartis Pharmaceuticals Corporation; Pfizer Inc.; Piramal Imaging;
522 Servier; Takeda Pharmaceutical Company; and Transition Therapeutics. The Canadian Institutes of Health
523 Research is providing funds to support ADNI clinical sites in Canada. Private sector contributions are
524 facilitated by the Foundation for the National Institutes of Health (www.fnih.org). The grantee organization

is the Northern California Institute for Research and Education, and the study is coordinated by the Alzheimer's Disease Cooperative Study at the University of California, San Diego. ADNI data are disseminated by the Laboratory for Neuro Imaging at the University of Southern California

## Author Contributions

J.W.V. and R.O. conceptualized and designed the study. P.S., A.C.E., O.H. and R.O. supervised the study. J.W.V., N.M., Y.I.M., T.O.S., M.S., P.B., O.H. and R.O. acquired, processed and analyzed the data. J.W.V., W.F. and R.O. drafted the manuscript. All authors provide critical or conceptual support and revised the manuscript.

## Potential Conflicts of Interest

OH has acquired research support (for the institution) from Roche, GE Healthcare, Biogen, AVID Radiopharmaceuticals, Fujirebio, and Euroimmun. In the past 2 years, he has received consultancy/speaker fees (paid to the institution) from Lilly, Roche, and Fujirebio. Many of these companies are involved in creating tau-PET radioligands, including AVID, who provided the ligands for this study.

American Psychiatric Association T (2013): Diagnostic and statistical manual of mental disorders : DSM-5. Fifth edition. Arlington, VA : American Psychiatric Association, [2013]. https://search.library.wisc.edu/catalog/9910187853902121.

Arriagada P V, Growdon JH, Hedleywhyte ET, Hyman BT (1992): Neurofibrillary Tangles But Not Senile Plaques Parallel Duration and Severity of Alzheimers-Disease. Neurology 42:631–639.

Bejanin A, Schonhaut DR, Joie R La, Kramer JH, Baker SL, Sosa N, Ayakta N, Cantwell A, Janabi M, Lauriola M, O 'neil JP, Gorno-Tempini ML, Miller ZA, Rosen HJ, Miller BL, Jagust WJ, Rabinovici GD (2017): Tau pathology and neurodegeneration contribute to cognitive impairment in Alzheimer's disease. Brain:1–15. https://watermark.silverchair.com/awx243.pdf?token=AQECAHi208BE49Ooan9kkhW_Ercy7Dm3ZL_9Cf3qfKAc485ysgAAAecwggHjBgkqhkiG9w0BBwagggHUMIIB0AIBADCCAckGCSqGSIb3DQEHATAeBglghkgBZQMEAS4wEQQM-3OjnBKCYybpS8fEAgEQgIIBmpY9paVgrJr248NQgNg8LAw6UHj7Y8NzZqCqEKPxMOE1DebS.

Bellec P (2013): Mining the hierarchy of resting-state brain networks: Selection of representative clusters in a multiscale structure. Proc - 2013 3rd Int Work Pattern Recognit Neuroimaging, PRNI 2013:54–57.

Bellec P, Perlbarg V, Jbabdi S, Pélégrini-Issac M, Anton JL, Doyon J, Benali H (2006): Identification of large-scale networks in the brain using fMRI. Neuroimage 29:1231–1243.

Bellec P, Rosa-Neto P, Lyttelton OC, Benali H, Evans AC (2010): Multi-level bootstrap analysis of stable clusters in resting-state fMRI. Neuroimage 51:1126–1139. http://dx.doi.org/10.1016/j.neuroimage.2010.02.082.

Braak H, Braak E (1991): Neuropathological stageing of Alzheimer-related changes. Acta Neuropathol 82:239–59. http://www.ncbi.nlm.nih.gov/pubmed/1759558.

Chien DT, Bahri S, Szardenings AK, Walsh JC, Mu F, Su M-Y, Shankle WR, Elizarov A, Kolb HC (2013): Early Clinical PET Imaging Results with the Novel PHF-Tau Radioligand [F-18]-T807. J Alzheimer's Dis 34:457–468.

Cho H, Choi JY, Hwang MS, Kim YJ, Lee HM, Lee HS, Lee JH, Ryu YH, Lee MS, Lyoo CH (2016): In vivo cortical spreading pattern of tau and amyloid in the Alzheimer's disease spectrum. Ann Neurol:1–12. http://doi.wiley.com/10.1002/ana.24711.

Cho H, Choi JY, Lee SH, Lee JH, Choi YC, Ryu YH, Lee MS, Lyoo CH (2017): Excessive tau accumulation in the parieto-occipital cortex characterizes early-onset Alzheimer's disease. Neurobiol Aging 53:103–111. http://dx.doi.org/10.1016/j.neurobiolaging.2017.01.024.

Choi JY, Cho H, Ahn SJ, Lee JH, Ryu YH, Lee MS, Lyoo CH (2017): "Off-Target" $^{18}$F-AV-1451 Binding in the Basal Ganglia Correlates with Age-Related Iron Accumulation. J Nucl Med:jnumed.117.195248. http://jnm.snmjournals.org/lookup/doi/10.2967/jnumed.117.195248.

Desikan RS, Ségonne F, Fischl B, Quinn BT, Dickerson BC, Blacker D, Buckner RL, Dale AM, Maguire RP, Hyman BT, Albert MS, Killiany RJ (2006): An automated labeling system for subdividing the human cerebral cortex on MRI scans into gyral based regions of interest. Neuroimage 31:968–980.

Dickerson BC, Stoub TR, Shah RC, Sperling RA, Killiany RJ, Albert MS, Hyman BT,

Blacker D, Detoledo-Morrell L (2011): Alzheimer-signature MRI biomarker predicts AD dementia in cognitively normal adults. Neurology 76:1395–1402.

Farias ST, Mungas D, Reed BR, Cahn-Weiner D, Jagust W, Baynes K, Decarli C (2008): The measurement of everyday cognition (ECog): scale development and psychometric properties. Neuropsychology 22:531–44. http://www.ncbi.nlm.nih.gov/pubmed/18590364.

Folstein MF, Folstein SE, McHugh PR (1975): "Mini-mental state". A practical method for grading the cognitive state of patients for the clinician. J Psychiatr Res 12:189–98. http://dx.doi.org/10.1016/0022-3956(75)90026-6.

Frisoni GB, Boccardi M, Barkhof F, Blennow K, Cappa S, Chiotis K, Démonet J-F, Garibotto V, Giannakopoulos P, Gietl A, Hansson O, Herholz K, Jack CR, Nobili F, Nordberg A, Snyder HM, Ten Kate M, Varrone A, Albanese E, Becker S, Bossuyt P, Carrillo MC, Cerami C, Dubois B, Gallo V, Giacobini E, Gold G, Hurst S, Lönneborg A, Lovblad K-O, Mattsson N, Molinuevo J-L, Monsch AU, Mosimann U, Padovani A, Picco A, Porteri C, Ratib O, Saint-Aubert L, Scerri C, Scheltens P, Schott JM, Sonni I, Teipel S, Vineis P, Visser PJ, Yasui Y, Winblad B (2017): Strategic roadmap for an early diagnosis of Alzheimer's disease based on biomarkers. Lancet Neurol 16:661–676. http://www.ncbi.nlm.nih.gov/pubmed/28721928.

Garcia-Garcia M, Nikolaidis A, Bellec P, Craddock RC, Cheung B, Castellanos FX, Milham MP (2017): Detecting stable individual differences in the functional organization of the human basal ganglia. Neuroimage:1–15. http://linkinghub.elsevier.com/retrieve/pii/S1053811917305979.

Hansson O, Grothe MJ, Strandberg TO, Ohlsson T (2017): Tau Pathology Distribution in Alzheimer ' s disease Corresponds Differentially to Cognition-Relevant Functional Brain Networks 11.

Harada R, Ishiki A, Kai H, Sato N, Furukawa K, Furumoto S, Tago T, Tomita N, Watanuki S, Hiraoka K, Ishikawa Y, Funaki Y, Nakamura T, Yoshikawa T, Iwata R, Tashiro M, Sasano H, Kitamoto T, Yanai K, Arai H, Kudo Y, Okamura N (2017): Correlations of (18)F-THK5351 PET with post-mortem burden of tau and astrogliosis in Alzheimer's disease. J Nucl Med. http://jnm.snmjournals.org/content/early/2017/08/31/jnumed.117.197426.abstract.

Hoenig MC, Bischof GN, Hammes J, Faber J, Fliessbach K, van Eimeren T, Drzezga A (2017): Tau pathology and cognitive reserve in Alzheimer's disease. Neurobiol Aging 57:1–7. http://dx.doi.org/10.1016/j.neurobiolaging.2017.05.004.

Hughes CP, Berg L, Danziger WL, Coben LA, Martin RL (1982): A new clinical scale for the staging of dementia. Br J Psychiatry 140:566–72. http://www.ncbi.nlm.nih.gov/pubmed/7104545.

Ikonomovic MD, Abrahamson EE, Ph D, Price JC, Ph D, Mathis CA, Ph D, Klunk WE, Ph D [ F-18 ] AV-1451 PET retention in choroid plexus : more than " off-target " binding:2–6.

Jansen WJ, Ossenkoppele R, Knol DL, Tijms BM, Scheltens P, Verhey FRJ, Visser PJ, Aalten P, Aarsland D, Alcolea D, Alexander M, Almdahl IS, Arnold SE, Baldeiras I, Barthel H, van Berckel BNM, Bibeau K, Blennow K, Brooks DJ, van Buchem MA, Camus V, Cavedo E, Chen K, Chetelat G, Cohen AD, Drzezga A, Engelborghs S, Fagan AM, Fladby T, Fleisher AS, van der Flier WM, Ford L, Förster S, Fortea J,

633 Foskett N, Frederiksen KS, Freund-Levi Y, Frisoni GB, Froelich L, Gabryelewicz T,
634 Gill KD, Gkatzima O, Gómez-Tortosa E, Gordon MF, Grimmer T, Hampel H,
635 Hausner L, Hellwig S, Herukka S-K, Hildebrandt H, Ishihara L, Ivanoiu A, Jagust
636 WJ, Johannsen P, Kandimalla R, Kapaki E, Klimkowicz-Mrowiec A, Klunk WE,
637 Köhler S, Koglin N, Kornhuber J, Kramberger MG, Van Laere K, Landau SM, Lee
638 DY, de Leon M, Lisetti V, Lleó A, Madsen K, Maier W, Marcusson J, Mattsson N,
639 de Mendonça A, Meulenbroek O, Meyer PT, Mintun MA, Mok V, Molinuevo JL,
640 Møllergård HM, Morris JC, Mroczko B, Van der Mussele S, Na DL, Newberg A,
641 Nordberg A, Nordlund A, Novak GP, Paraskevas GP, Parnetti L, Perera G, Peters O,
642 Popp J, Prabhakar S, Rabinovici GD, Ramakers IHGB, Rami L, Resende de Oliveira
643 C, Rinne JO, Rodrigue KM, Rodríguez-Rodríguez E, Roe CM, Rot U, Rowe CC,
644 Rüther E, Sabri O, Sanchez-Juan P, Santana I, Sarazin M, Schröder J, Schütte C,
645 Seo SW, Soetewey F, Soininen H, Spiru L, Struyfs H, Teunissen CE, Tsolaki M,
646 Vandenberghe R, Verbeek MM, Villemagne VL, Vos SJB, van Waalwijk van Doorn
647 LJC, Waldemar G, Wallin A, Wallin ÅK, Wiltfang J, Wolk DA, Zboch M,
648 Zetterberg H (2015): Prevalence of Cerebral Amyloid Pathology in Persons Without
649 Dementia: A Meta-analysis. Jama 313:1924–1938.
650 http://www.pubmedcentral.nih.gov/articlerender.fcgi?artid=4486209&tool=pmcentr
651 ez&rendertype=abstract.
652 Johnson KA, Schultz A, Betensky RA, Becker JA, Sepulcre J, Rentz D, Mormino E,
653 Chhatwal J, Amariglio R, Papp K, Marshall G, Albers M, Mauro S, Pepin L, Alverio
654 J, Judge K, Philiossaint M, Shoup T, Yokell D, Dickerson B, Gomez-Isla T, Hyman
655 B, Vasdev N, Sperling R (2016): Tau positron emission tomographic imaging in
656 aging and early Alzheimer disease. Ann Neurol 79:110–119.
657 Jones DT, Graff-Radford J, Lowe VJ, Wiste HJ, Gunter JL, Senjem ML, Botha H,
658 Kantarci K, Boeve BF, Knopman DS, Petersen RC, Jack CR (2017): Tau, Amyloid,
659 and Cascading Network Failure across the Alzheimer's disease Spectrum. Cortex:1–
660 17. http://linkinghub.elsevier.com/retrieve/pii/S0010945217303246.
661 Landau SM, Harvey D, Madison CM, Koeppe RA, Reiman EM, Foster NL, Weiner MW,
662 Jagust WJ (2011): Associations between cognitive, functional, and FDG-PET
663 measures of decline in AD and MCI. Neurobiol Aging 32:1207–1218.
664 Landau SM, Lu M, Joshi AD, Pontecorvo M, Mintun MA, Trojanowski JQ, Shaw LM,
665 Jagust WJ (2013): Comparing positron emission tomography imaging and
666 cerebrospinal fluid measurements of ??-amyloid. Ann Neurol 74:826–836.
667 Lockhart SN, Ayakta N, Winer JR, La Joie R, Rabinovici GD, Jagust WJ (2017):
668 Elevated (18)F-AV-1451 PET tracer uptake detected in incidental imaging findings.
669 Neurology 88:1095–1097. http://www.ncbi.nlm.nih.gov/pubmed/28188303.
670 Lowe VJ, Curran G, Fang P, Liesinger AM, Josephs KA, Parisi JE, Kantarci K, Boeve
671 BF, Pandey MK, Bruinsma T, Knopman DS, Jones DT, Petrucelli L, Cook CN,
672 Graff-Radford NR, Dickson DW, Petersen RC, Jack CR, Murray ME (2016): An
673 autoradiographic evaluation of AV-1451 Tau PET in dementia. Acta Neuropathol
674 Commun 4:58. http://actaneurocomms.biomedcentral.com/articles/10.1186/s40478-
675 016-0315-6.
676 Maass A, Landau S, Baker SL, Horng A, Lockhart SN, La R, Rabinovici GD, Jagust WJ,
677 Initiative N (2017): NeuroImage Comparison of multiple tau-PET measures as
678 biomarkers in aging and Alzheimer ' s disease. Neuroimage 157:448–463.

http://dx.doi.org/10.1016/j.neuroimage.2017.05.058.
Marquié M, Normandin MD, Vanderburg CR, Costantino IM, Bien EA, Rycyna LG, Klunk WE, Mathis CA, Ikonomovic MD, Debnath ML, Vasdev N, Dickerson BC, Gomperts SN, Growdon JH, Johnson KA, Frosch MP, Hyman BT, Gómez-Isla T (2015): Validating novel tau positron emission tomography tracer [F-18]-AV-1451 (T807) on postmortem brain tissue. Ann Neurol 78:787–800. http://www.ncbi.nlm.nih.gov/pubmed/26344059.
Marquié M, Siao Tick Chong M, Antón-Fernández A, Verwer EE, Sáez-Calveras N, Meltzer AC, Ramanan P, Amaral AC, Gonzalez J, Normandin MD, Frosch MP, Gómez-Isla T (2017): [F-18]-AV-1451 binding correlates with postmortem neurofibrillary tangle Braak staging. Acta Neuropathol:1–10.
Masters CL, Simms G, Weinman NA, Multhaup G, McDonald BL, Beyreuther K (1985): Amyloid plaque core protein in Alzheimer disease and Down syndrome. Proc Natl Acad Sci U S A 82:4245–9. http://www.ncbi.nlm.nih.gov/pubmed/3159021%5Cnhttp://www.pubmedcentral.nih.gov/articlerender.fcgi?artid=PMC397973.
McKhann G, Knopman DS, Chertkow H, Hymann B, Jack CR, Kawas C, Klunk W, Koroshetz W, Manly J, Mayeux R, Mohs R, Morris J, Rossor M, Scheltens P, Carrillo M, Weintrub S, Phelphs C (2011): The diagnosis of dementia due to Alzheimer's disease: Recommendations from the National Institute on Aging-Alzheimer's Association workgroups on diagnostic guidelines for Alzheimer's disease. Alzheimers Dement 7:263–269.
Mishra S, Gordon BA, Su Y, Christensen J, Friedrichsen K, Jackson K, Hornbeck R, Balota DA, Cairns NJ, Morris JC, Ances BM, Benzinger TLS (2017): AV-1451 PET imaging of tau pathology in preclinical Alzheimer disease: Defining a summary measure. Neuroimage 161:171–178.
Mohs RC, Knopman D, Petersen RC, Ferris SH, Ernesto C, Grundman M, Sano M, Bieliauskas L, Geldmacher D, Clark C, Thal LJ (1997): Development of cognitive instruments for use in clinical trials of antidementia drugs: additions to the Alzheimer's Disease Assessment Scale that broaden its scope. The Alzheimer's Disease Cooperative Study. Alzheimer Dis Assoc Disord 11 Suppl 2:S13-21. http://www.ncbi.nlm.nih.gov/pubmed/9236948.
Nelson P. T. et al (2013): Correlation of Alzheimer Disease Neuropathologic Changes With Cognitive Status: A Review of the Literature. J Neuropathol Exp Neurol 2012 May ; 71(5) 362–381 doi101097/NEN0b013e31825018f7 71:362–381.
Ng KP, Pascoal TA, Mathotaarachchi S, Therriault J, Kang MS, Shin M, Guiot M-C, Guo Q, Harada R, Comley RA, Massarweh G, Soucy J-P, Okamura N, Gauthier S, Rosa-Neto P (2017): Monoamine oxidase B inhibitor, selegiline, reduces 18 F-THK5351 uptake in the human brain. Alzheimers Res Ther 9:25. http://content.wkhealth.com/linkback/openurl?sid=WKPTLP:landingpage&an=00001756-199808030-00031%5Cnhttp://download.springer.com/static/pdf/689/art%253A10.1186%252Fs13195-017-0253-y.pdf?originUrl=http%3A%2F%2Falzres.biomedcentral.com%2Farticle%2F10.1186%2F.
Ossenkoppele R, Schonhaut DR, Schöll M, Lockhart SN, Ayakta N, Baker SL, O'Neil

JP, Janabi M, Lazaris A, Cantwell A, Vogel J, Santos M, Miller ZA, Bettcher BM, Vossel KA, Kramer JH, Gorno-Tempini ML, Miller BL, Jagust WJ, Rabinovici GD (2016): Tau PET patterns mirror clinical and neuroanatomical variability in Alzheimer's disease. Brain 139:1551–1567. http://brain.oxfordjournals.org/.

Ota K, Oishi N, Ito K, Fukuyama H (2015): Effects of imaging modalities, brain atlases and feature selection on prediction of Alzheimer's disease. J Neurosci Methods 256:168–183.

Palmqvist S, Zetterberg H, Mattsson N, Johansson P, Minthon L, Blennow K, Olsson M, Hansson O (2015): Detailed comparison of amyloid PET and CSF biomarkers for identifying early Alzheimer disease. Neurology 85:1240–1249.

Pankov A, Binney RJ, Staffaroni AM, Kornak J, Attygalle S, Schuff N, Weiner MW, Kramer JH, Dickerson BC, Miller BL, Rosen HJ (2016): Data-driven regions of interest for longitudinal change in frontotemporal lobar degeneration. NeuroImage Clin 12:332–340. http://dx.doi.org/10.1016/j.nicl.2015.08.002.

Pedregosa F, Varoquaux G, Gramfort A, Michel V, Thirion B, Grisel O, Blondel M, Louppe G, Prettenhofer P, Weiss R, Dubourg V, Vanderplas J, Passos A, Cournapeau D, Brucher M, Perrot M, Duchesnay É (2012): Scikit-learn: Machine Learning in Python. J Mach Learn Res 12:2825–2830. http://arxiv.org/abs/1201.0490.

Pfeffer RI, Kurosaki TT, Harrah CH, Chance JM, Filos S (1982): Measurement of functional activities in older adults in the community. J Gerontol 37:323–9. http://www.ncbi.nlm.nih.gov/pubmed/7069156.

Rosen WG, Mohs RC, Davis KL (1984): A new rating scale for Alzheimer's disease. Am J Psychiatry 141:1356–1364,.

Van Rossum IA, Visser PJ, Knol DL, Van Der Flier WM, Teunissen CE, Barkhof F, Blankenstein MA, Scheltens P (2012): Injury markers but not amyloid markers are associated with rapid progression from mild cognitive impairment to dementia in alzheimer's disease. J Alzheimer's Dis 29:319–327.

Scheltens P, Rockwood K (2011): How golden is the gold standard of neuropathology in dementia? Alzheimer's Dement 7:486–489. http://dx.doi.org/10.1016/j.jalz.2011.04.011.

Schöll M, Lockhart SN, Schonhaut DR, O'Neil JP, Janabi M, Ossenkoppele R, Baker SL, Vogel JW, Faria J, Schwimmer HD, Rabinovici GD, Jagust WJ (2016): PET Imaging of Tau Deposition in the Aging Human Brain. Neuron 89:971–982.

Schwarz AJ, Yu P, Miller BB, Shcherbinin S, Dickson J, Navitsky M, Joshi AD, Devous MD, Mintun MS (2016): Regional profiles of the candidate tau PET ligand $^{18}$F-AV-1451 recapitulate key features of Braak histopathological stages. Brain:aww023. http://www.brain.oxfordjournals.org/lookup/doi/10.1093/brain/aww023.

Sepulcre J, Grothe MJ, Sabuncu M, Chhatwal J, Schultz AP, Hanseeuw B, El Fakhri G, Sperling R, Johnson KA (2017): Hierarchical Organization of Tau and Amyloid Deposits in the Cerebral Cortex. JAMA Neurol 74:813. http://archneur.jamanetwork.com/article.aspx?doi=10.1001/jamaneurol.2017.0263.

Smith R, Schain M, Nilsson C, Strandberg O, Olsson T, Hägerström D, Jögi J, Borroni E, Schöll M, Honer M, Hansson O (2016): Increased Basal Ganglia Binding of 18F-AV-1451 in Patients With Progressive Supranuclear Palsy. Mov Disord 0:1–7.

Stern Y (2012): Cognitive reserve in ageing and Alzheimer's disease. Lancet Neurol

11:1006–1012. http://dx.doi.org/10.1016/S1474-4422(12)70191-6.

Weiner MW, Veitch DP, Aisen PS, Beckett LA, Cairns NJ, Green RC, Harvey D, Jack CR, Jagust W, Liu E, Morris JC, Petersen RC, Saykin AJ, Schmidt ME, Shaw L, Siuciak JA, Soares H, Toga AW, Trojanowski JQ (2012): The Alzheimer's disease neuroimaging initiative: A review of papers published since its inception. Alzheimer's Dement 8:S1–S68. http://dx.doi.org/10.1016/j.jalz.2011.09.172.

Xia C, Makaretz SJ, Caso C, McGinnis S, Gomperts SN, Sepulcre J, Gomez-Isla T, Hyman BT, Schultz A, Vasdev N, Johnson KA, Dickerson BC (2017): Association of In Vivo [ $^{18}$ F]AV-1451 Tau PET Imaging Results With Cortical Atrophy and Symptoms in Typical and Atypical Alzheimer Disease. JAMA Neurol 74:427. http://archneur.jamanetwork.com/article.aspx?doi=10.1001/jamaneurol.2016.5755.

Xia C-F, Arteaga J, Chen G, Gangadharmath U, Gomez LF, Kasi D, Lam C, Liang Q, Liu C, Mocharla VP, Mu F, Sinha A, Su H, Szardenings AK, Walsh JC, Wang E, Yu C, Zhang W, Zhao T, Kolb HC (2013): [18F]T807, a novel tau positron emission tomography imaging agent for Alzheimer's disease. Alzheimer's Dement 9:666–676. http://linkinghub.elsevier.com/retrieve/pii/S1552526012025320.

789 # FIGURES LEGENDS

790

791 **Figure 1. Mean [$^{18}$F]AV1451 uptake according to diagnosis, amyloid status and**

792 **cohort**

793 Mean [$^{18}$F]AV1451 SUVR images stratified by amyloid status and disease stage, across

794 both the ADNI (top) and BioFINDER (bottom) cohorts.

795

796 **Figure 2. Bootstrap analysis of stable clusters on [$^{18}$F]AV1451 data.** [$^{18}$F]AV1451

797 scans were entered into a voxelwise clustering algorithm. The optimal solutions were

798 determined using the M-STEPS approach. This resulted in five [$^{18}$F]AV1451 covariance

799 networks. These networks were masked with a stability threshold of 0.5, and are

800 displayed in the lower half of the figure.

801

802 **Figure 3. Comparison between data-driven and hypothesis-driven ROIs.** Data-driven

803 [$^{18}$F]AV1451 covariance networks were compared to previously existing Braak Stage

804 ROIs from the literature using descriptive statistics. The clusters were compared to ROIs

805 from Schöll, Lockhart et al. and Cho et al using Normalized Mutual Information (top

806 left), and were compared to regions from Schwarz et al. using the percentage of Schwarz

807 ROI voxels within each data-driven cluster.

808

809 **FIGURE 4. Associations between [$^{18}$F]AV1451 ROIs and global cognition.** General

810 linear models comparing [$^{18}$F]AV1451 signal to Global Cognition composite scores were

811 run, adjusting for age, sex and education. For each model, a different [$^{18}$F]AV1451 ROI

812 was used. ROIs included the five clusters identified in our analysis, as well as Braak

813 stage regions taken from three different papers: Schöll, Lockhart et al., 2016 *Neuron*; Cho
814 et al., 2016 *Ann. Neurol.*; Schwarz et al., 2016 *Brain*. Two versions of each Braak ROI
815 were created, one using regions from that stage only (e.g. Stage 3), and one combining all
816 regions from that stage with all regions from previous stages (e.g. Stage 1+2+3). The
817 effect size (t-value) of each tau ROI is shown. AV1451 binding in several ROIs
818 demonstrated strong relationships with Global Cognition, though only the data-driven
819 Temporo-parietal region survived multiple comparisons.
820
821 **Figure 5. Cumulative ranking of ROI performance across all measures of global**
822 **cognition and function.** For each measure of global cognition, [$^{18}$F]AV1451 ROIs were
823 ranked from worst to best (such that the worst region would have rank of 1) with respect
824 to the effect size of the association between [$^{18}$F]AV1451 in that region and the cognitive
825 score. The ranks were then summed across all cognitive measurements and are displayed
826 here. The data-driven Cluster 4 ("Temporo-parietal") ranked the best cumulatively across
827 cognitive tests, with the data-driven Cluster 3 ("Medial/Inferior/Anterior temporal")
828 ranking second best.
829
830 **FIGURE 6. Lasso regression selects most important features related to cognition.**
831 All [$^{18}$F]AV1451 ROIs plus age, sex and education were entered into a L1-penalized
832 Lasso regression feature selection routine with the Global Cognitive composite score as
833 the dependent variable. The Lasso selected education and two ROIs: the data-driven
834 Temporo-parietal region, and the Schwarz Single VI region. Together in a general linear
835 model, these features explained 28% of the variance in the Global Cognition score.
836

# TABLES

**Table 1: Demographic information, MMSE scores and amyloid-positivity rates**

| | Controls | | MCI | | AD | | Total | |
|---|---|---|---|---|---|---|---|---|
| | **BioF** | **ADNI** | **BioF** | **ADNI** | **BioF** | **ADNI** | **BioF** | **ADNI** |
| **n** | 55 | 43 | 21 | 37 | 47 | 10 | 123 | 90 |
| **Age (SD)** | **75.0 (6.2)** | **70.3 (5.9)** | 70.8 (10.9) | 72.0 (6.8) | 70.1 (8.6) | 73.3 (4.3) | 72.4 (8.4) | 71.3 (6.1) |
| **% Male** | 50.9% | 46.5% | 57.1% | 67.6% | 55.3% | 60.0% | 53.7% | 56.7% |
| **Education (SD)** | **12.0 (3.7)** | **16.1 (2.4)** | **11.7 (3.7)** | **16.9 (2.7)** | **12.2 (3.2)** | **15.0 (3.0)** | **12.0 (3.5)** | **16.3 (2.6)** |
| **% Amyloid+** | 43.6% | 33.3% | **100%** | **44%** | 100% | 100% | **73.3%** | **44.8%** |
| **MMSE (SD)** | 29.1 (1.1) | 29.0 (1.3) | **25.7 (2.8)** | **28.4 (2.0)** | **21.2 (5.1)** | **25.5 (5.1)** | **25.5 (4.9)** | **28.3 (2.5)** |

- * **BOLD** text indicates significant difference ($p<0.05$) between cohorts, as measured by t-test, or Fisher's Exact Tests
- ADNI = Alzheimer's Disease Neuroimaging Initiative; BioF = BioFINDER, MMSE = Mini-Mental State Examination; SD = Standard Deviation

# FIGURES

Figure 1

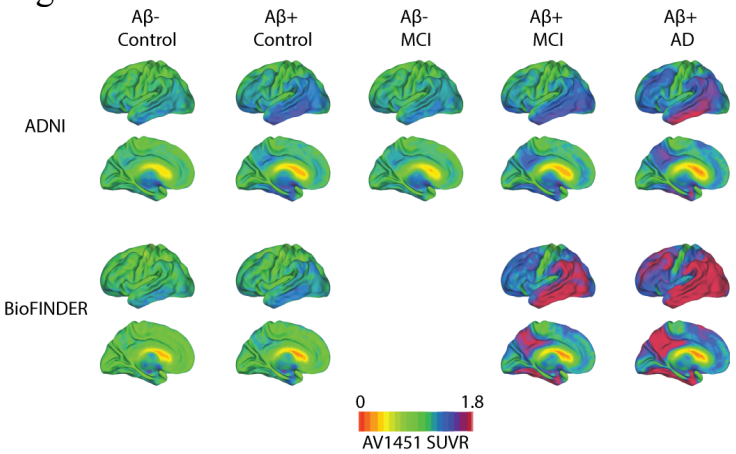


Figure 2

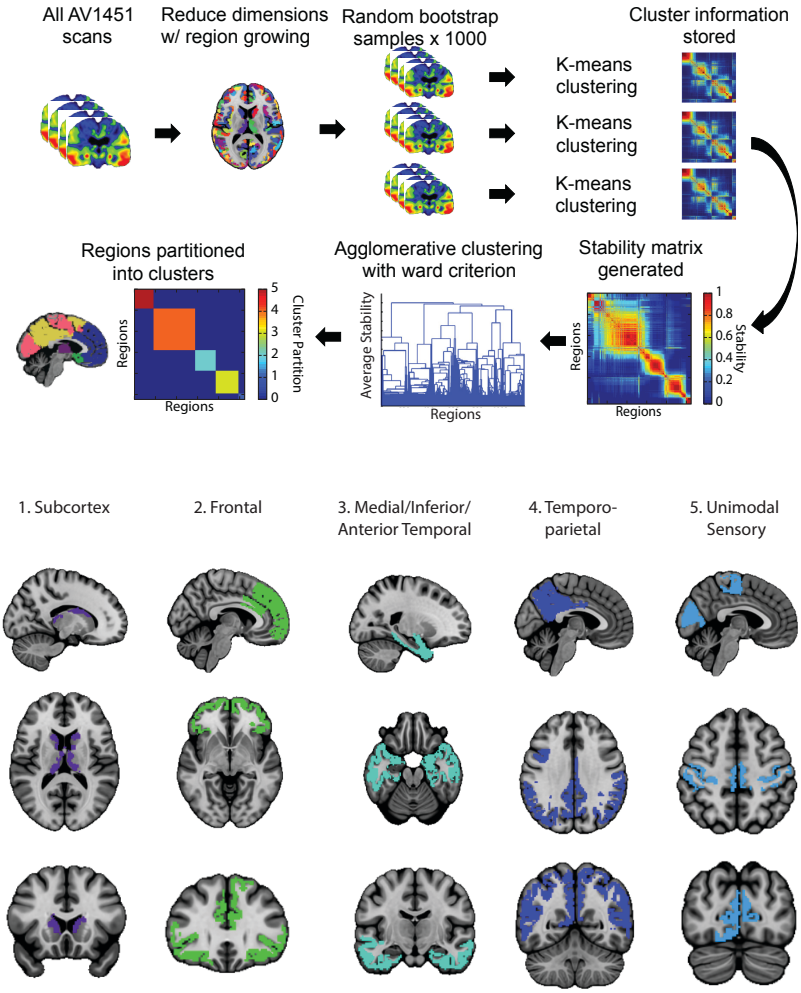

Figure 3

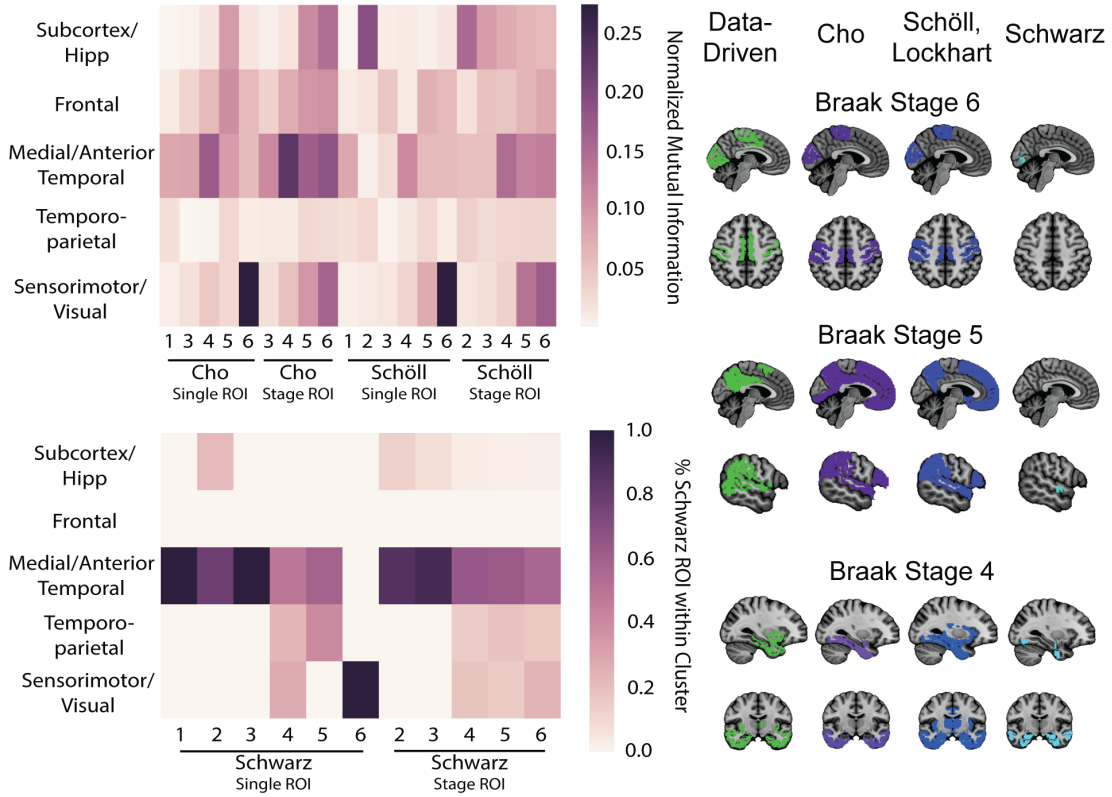


Figure 4

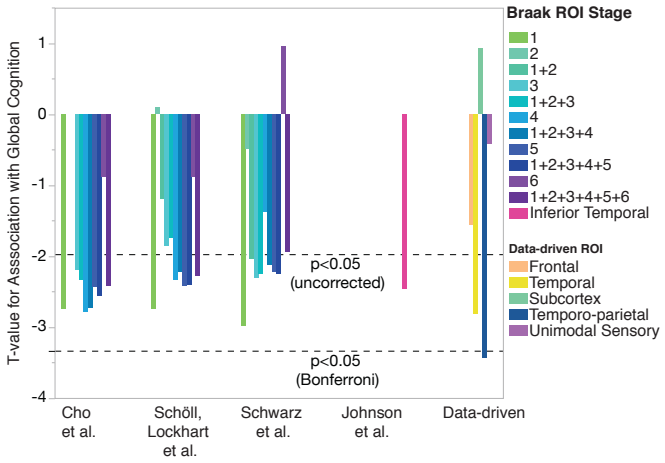

Figure 5

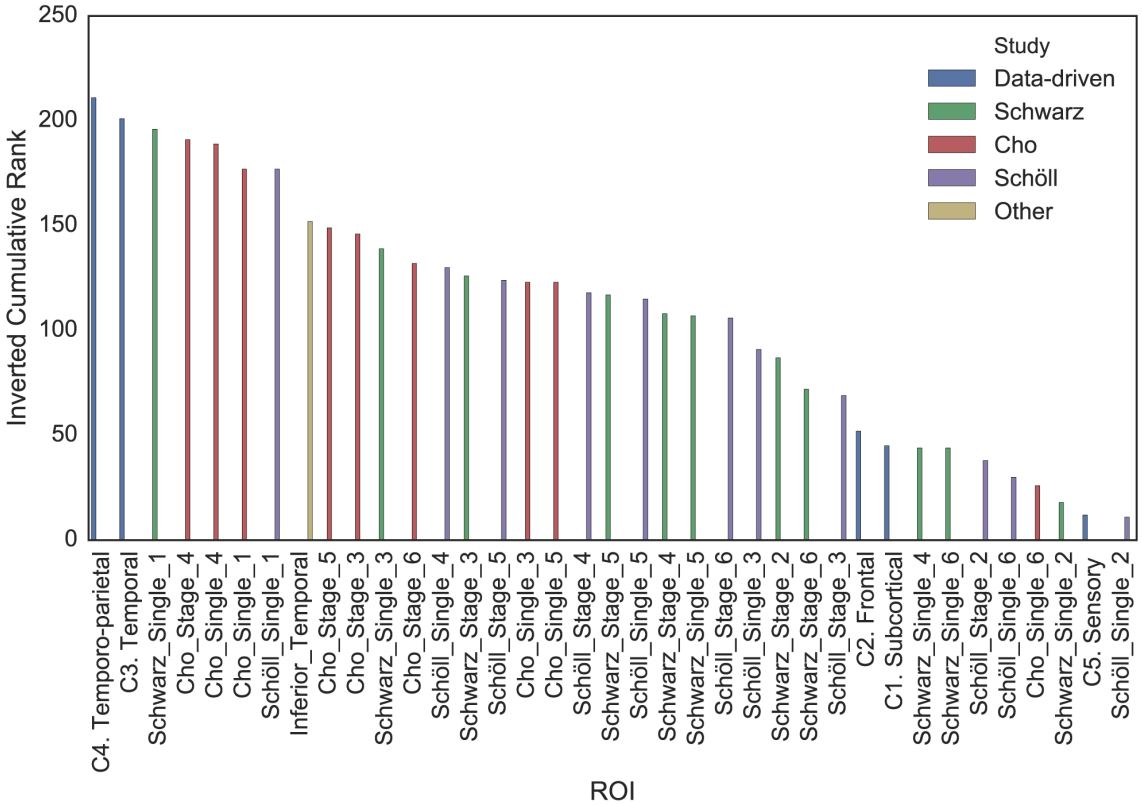


Figure 6

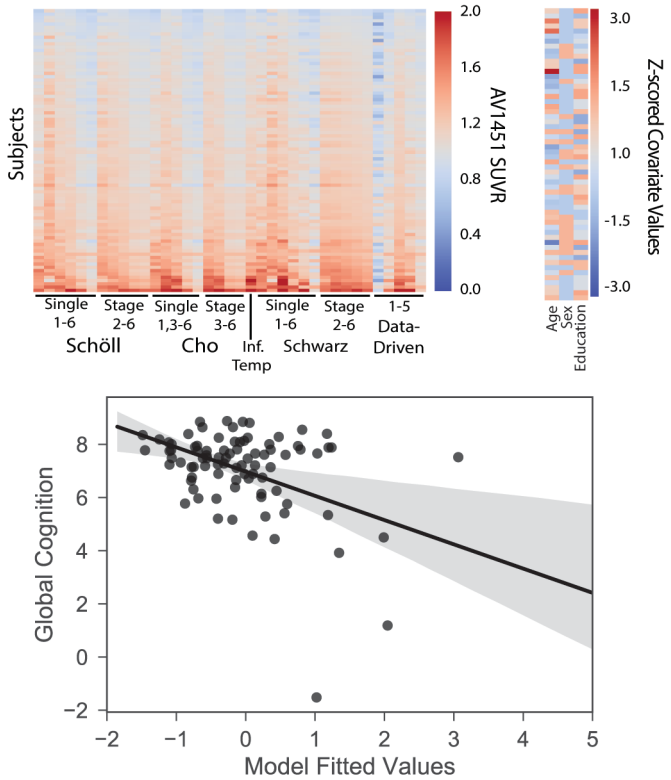

885 **SUPPLEMENTARY**

886

887 **Table S1. Best-ranking AV1451 ROIs at describing global cognition across different**
888 **cognitive tests**

| | MMSE | | | CDRSB | | |
|---|---|---|---|---|---|---|
| **Rank** | **Study** | **ROI** | **t** | **Study** | **ROI** | **t** |
| **1** | Data-driven | Temporo-parietal | -2.45* | Schwarz | Stage I | 3.60** |
| **2** | Data-driven | Temporal | -2.00* | Data-driven | Temporo-parietal | 3.49** |
| **3** | Cho | Single IV | -1.97 | Cho/Scholl | Stage I | 3.49** |
| **4** | Cho | Stage IV | -1.83 | Data-driven | Temporal | 3.33** |
| **5** | Other | Inferior Temporal | -1.80 | Cho | Stage IV | 3.18* |

| | ADAS11 | | | ADAS13 | | |
|---|---|---|---|---|---|---|
| **Rank** | **Study** | **ROI** | **t** | **Study** | **ROI** | **t** |
| **1** | Data-driven | Temporo-parietal | 4.10** | Data-driven | Temporo-parietal | 3.02* |
| **2** | Schwarz | Stage I | 3.50** | Schwarz | Stage I | 2.57* |
| **3** | Cho | Single IV | 3.43** | Data-Driven | Temporal | 2.35* |
| **4** | Data-driven | Temporal | 3.39** | Cho/Scholl | Stage I | 2.34* |
| **5** | Cho | Stage IV | 3.33** | Cho | Single IV | 2.34* |

| | ECOG | | | FAQ | | |
|---|---|---|---|---|---|---|
| **Rank** | **Study** | **ROI** | **t** | **Study** | **ROI** | **t** |
| **1** | Data-driven | Temporo-parietal | 3.68** | Schwarz | Stage I | 2.91* |
| **2** | Cho | Stage IV | 3.48** | Data-driven | Temporal | 2.69* |
| **3** | Schwarz | Stage I | 3.40** | Cho/Scholl | Stage I | 2.68* |
| **4** | Cho | Single IV | 3.40** | Data-driven | Temporo-parietal | 2.67* |
| **5** | Data-Driven | Temporal | 3.40** | Cho | Stage III | 2.63* |

889 * $p<0.05$ ** $p[Bonf.]<0.05$
890 ROI = Region of Interest; MMSE = Mini-Mental State Examination; CDRSB = Clinical
891 Dementia Rating Sum of Boxes; ADAS = Alzheimer's disease Assessment Scale; ECog
892 = Everyday Cognition; FAQ = Functional Activities Questionnaire
893
894
895
896
897
898

**Table S2. Fitted values from the General Linear Model comparing selected AV1451 ROIs to Global Cognition composite also explains variance in individual cognitive tests.**

| Test | $R^2$ |
|---|---|
| CDRSB | 0.214 |
| ADAS11 | 0.261 |
| ADAS13 | 0.215 |
| FAQ | 0.221 |
| ECog | 0.196 |
| MMSE | 0.219 |

MMSE = Mini-Mental State Examination; CDRSB = Clinical Dementia Rating Sum of Boxes; ADAS = Alzheimer's disease Assessment Scale; ECog = Everyday Cognition; FAQ = Functional Activities Questionnaire

**Table S3. Variables selected by Lasso regression that optimally described global cognition across different cognitive tests**

| MMSE | | CDRSB | | ADA |
|---|---|---|---|---|
| **Study** | **ROI** | **Study** | **ROI** | **Study** |
| Data-driven | Temporo-parietal | Data-driven | Temporo-parietal | Data-driven |
| Data-driven | Subcortical | | | Schwarz |
| Schwarz | Stage VI | | | Schwarz |
| Demographic | Education | | | Demographic |

| ADAS13 | | ECOG | | FA |
|---|---|---|---|---|
| **Study** | **ROI** | **Study** | **ROI** | **Study** |
| Data-driven | Temporo-parietal | Data-driven | Temporo-parietal | Data-driven |
| Schwarz | Single VI | | | Schwarz |
| Schwarz | Stage I | | | Schwarz |
| Schöll | Single II | | | Demographic |
| Demographic | Education | | | |
| Demographic | Age | | | |

MMSE = Mini-Mental State Examination; CDRSB = Clinical Dementia Rating Sum of Boxes; ADAS = Alzheimer's disease Assessment Scale; ECog = Everyday Cognition; FAQ = Functional Activities Questionnaire

**Table S4. Disparities in Braak stage regions-of-interests across studies**

| Brain Region | Schöll, Lockhart et al. | Cho et al. | Schwarz et al. | Data-driven |
|---|---|---|---|---|
| **Hippocampus** | Included | Not included | Head only | Head only |
| **Lingual Gyrus** | Stage 3 | Stage 5 | Stage 6 | TP/US |
| **Thalamus** | Stage 4 | Not included | Not Included | SCN |
| **Putamen** | Stage 5 | Not included | Not Included | MAIT |
| **Lateral Occipital** | Stage 5 | Stage 5 | Stage 4 | TP/US |
| **PCC** | Stage 4 | Stage 5 | Not Included | TP |
| **Insula** | Stage 4 | Stage 5 | Not Included | MAIT |
| **Frontal Lobe** | All stage 5 | All stage 5 | Not Included | F/TP |

TP = Temporo-parietal; US = Unimodal Sensory; SCN = Subcortical/Noise; MAIT = Medial/Anterior/Inferior Temporal; F = Frontal